Figure S1.

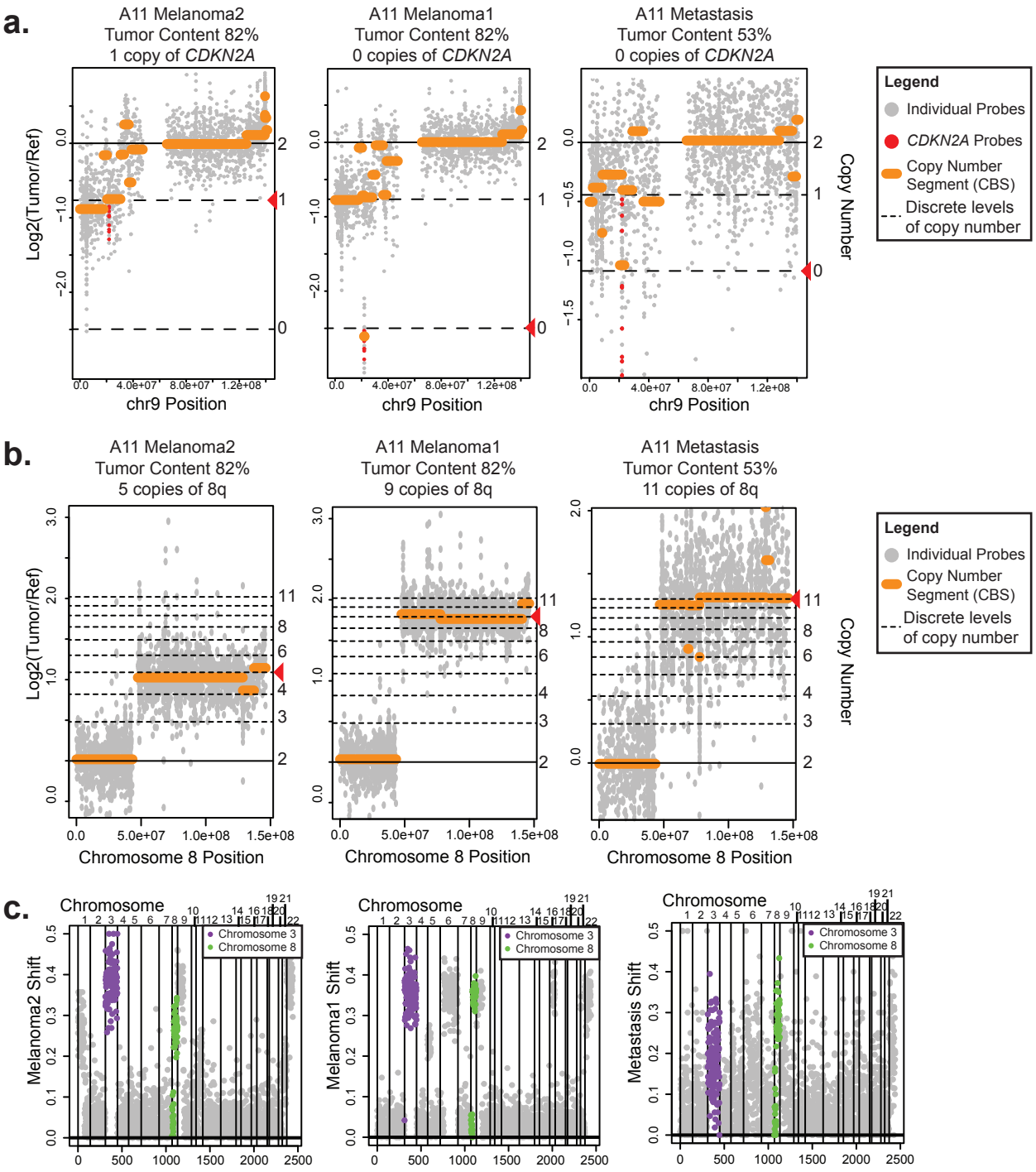

Figure S1. Stepwise deletion of *CDKN2A* and stepwise amplification of chromosomal arm 8q in case A11. a-b. Probe-level copy number data for chromosome 9 (panel a) and chromosome 8 (panel b) in all melanoma regions from case A11. Log-scale ratios are shown on the y-axis (left side), but due to differences in tumor cellularity, these values are not comparable across tumors. We therefore also show absolute levels of copy number on the y-axis (right side) with extended dotted lines for each discrete level. Note the stepwise loss of *CDKN2A* -- 1 copy in melanoma2 and 0 copies in melanoma1 and the metastasis. Also note the stewise gain of chromosomal arm 8q -- 5 copies in Mel2, 9 copies in Mel1, and 11 copies in the metastasis. **c.** Allelic imbalance, plotted on the y-axis as the deviation from a 0.5:0.5 split of reads, at each heterozygous SNP ordered by position across the genome (x-axis). Note that allelic imbalance corroborates the copy number alterations shown in figure 1c, including CNAs on chromosomes 3 and 8q (highlighted).

Figure S2.

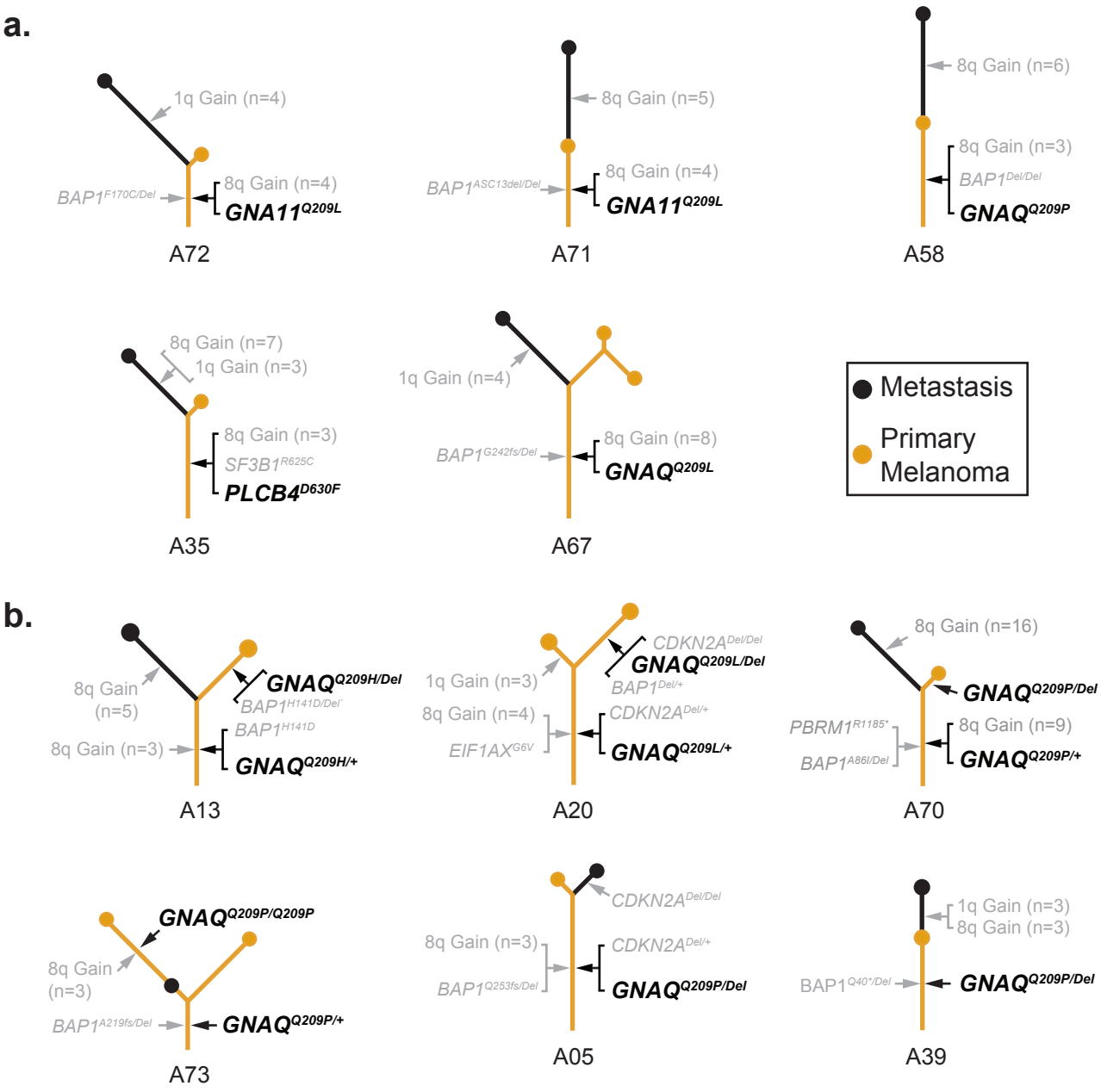

Figure S2. Gain-of-function mutations in the Gq signaling cascade are ubiquitous and undergo early selection; loss of wild-type *GNAQ* occurs later in a subset of uveal melanomas. a. Examples of phylogenetic trees in which gain-of-function mutations in the Gq signaling cascade (highlighted in **bold**) underwent selection comparatively early (indicated by their truncal position). **b.** Examples of phylogenetic trees in which *GNAQ* mutations become hemi- or homo- zygous comparatively later (indicated by their branchial position in 4/6 trees). These events were exclusive to *GNAQ* (*GNA11* mutations never underwent loss-of-heterozygosity in our cohort). The detailed evolution of each case is available in the supplementary dataset (see Methods).

Figure S3.

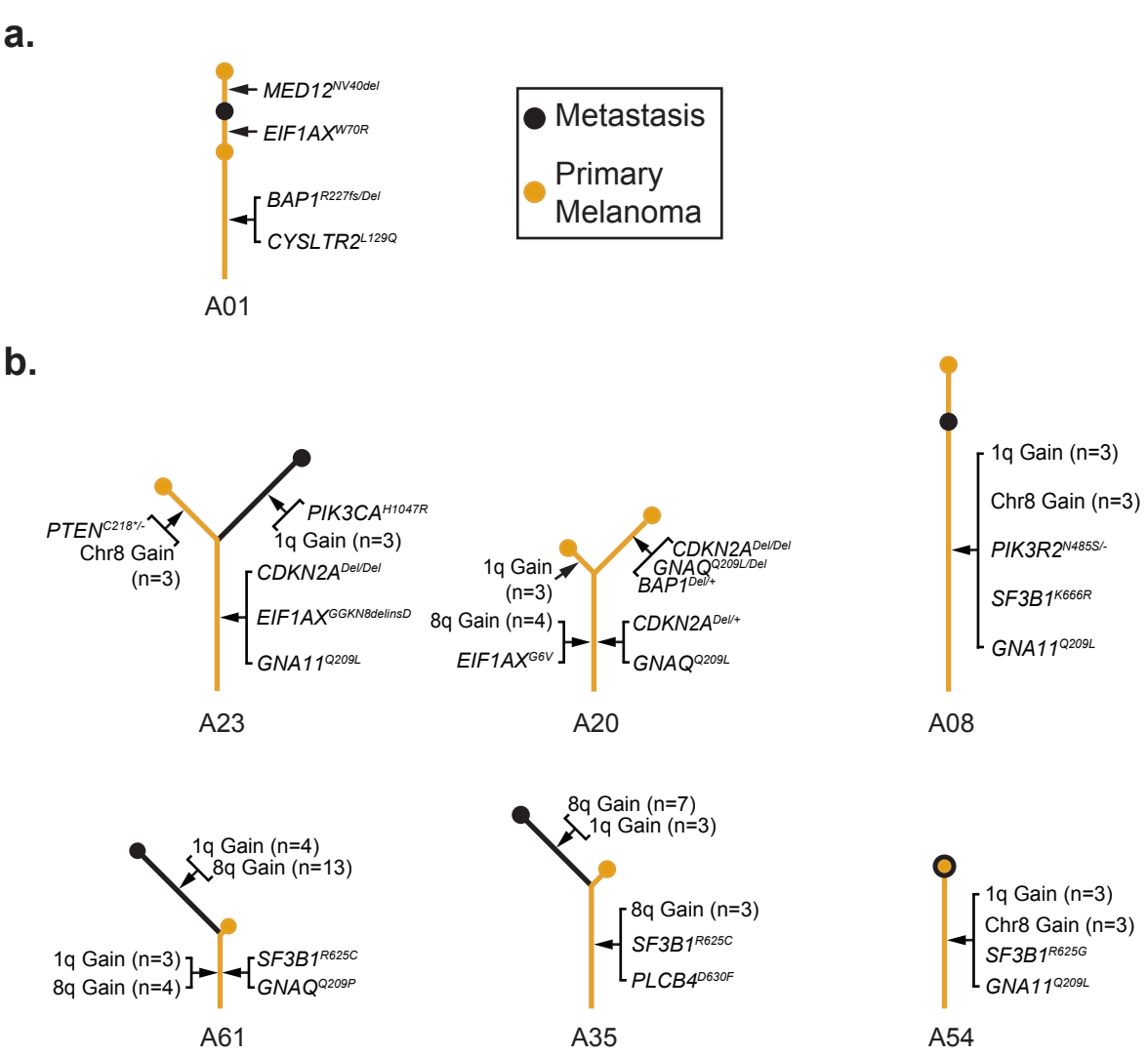

Figure S3. *SF3B1*- and *EIF1AX*- mutant uveal melanomas acquire additional oncogenic mutations. a. An example of an *EIF1AX* mutation occurring in conjuction with bi-allelic *BAP1* mutations. As discussed, we distinguished this case from the 'true' *SF3B1*- and *EIF1AX*-driven tumors shown in panel b, though notably this case acquired a $MED12^{NV40del}$ -- a mutation not previously reported in uveal melanoma. **b.** Examples of 'true' *EIF1AX*- or *SF3B1*- driven uveal melanomas. Several of these uveal melanomas acquired additional pathogenic mutations during the course of evolution, including alterations not known to occur in uveal melanoma, such as PI3-kinase pathway mutations (Case A23 and A08) and bi-allelic *CDKN2A* alterations (Case A23 and A20).

Figure S4.

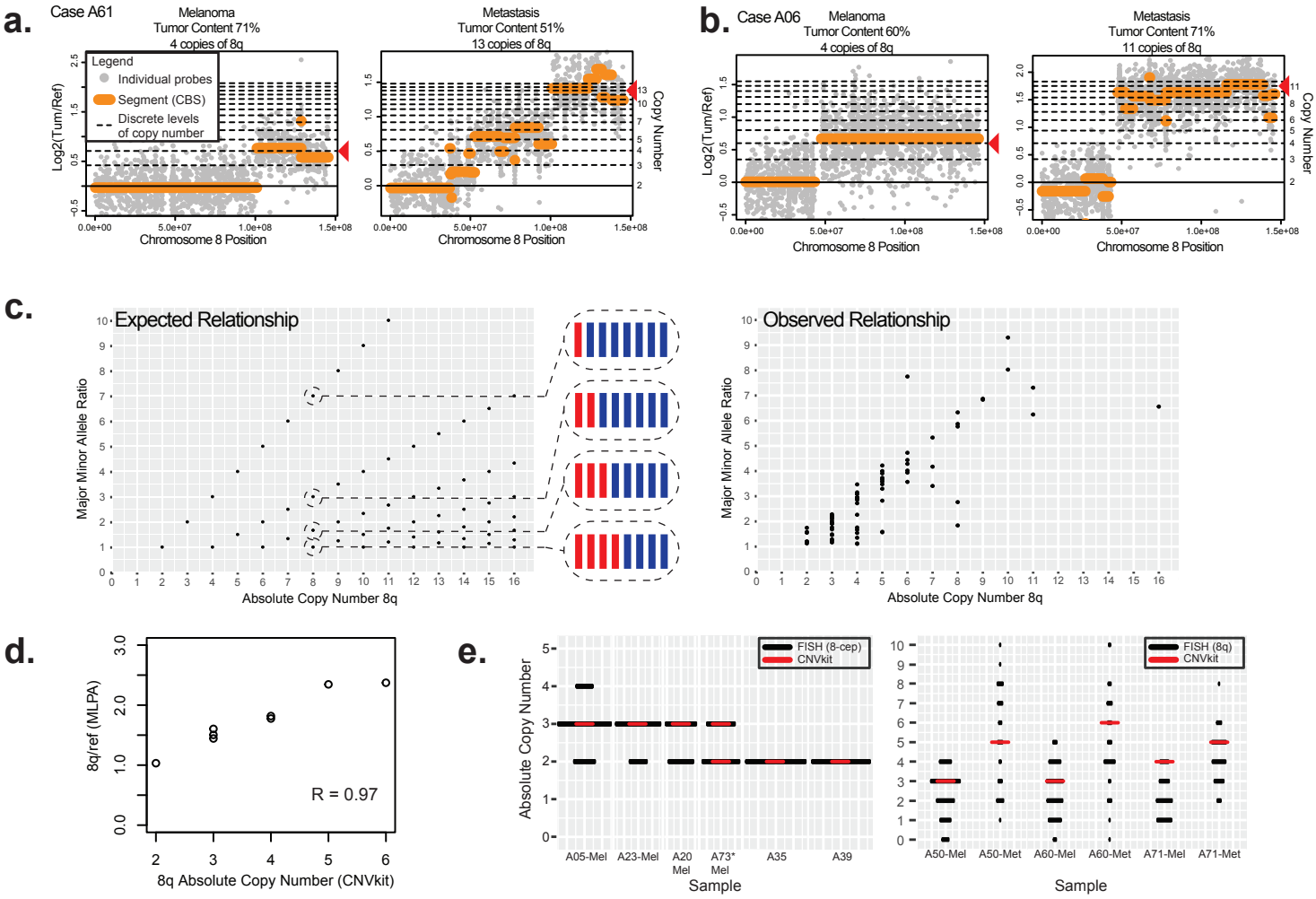

Figure S4. Copy number inference over chromosomal arm 8q. a-b. Probe level copy number data for chromosome 8 in Case A61 (panel a) and Case A06 (panel b). Log-scale ratios are shown on the y-axis (left side), but due to differences in tumor cellularity, these values are not comparable across tumors. Absolute levels of copy number are shown (right side) and are comparable across tumors. **c.** Correlation between absolute copy number and allelic imbalance over chromosomal arm 8q. Absolute copy number was inferred from the amplitude of gain over chromosome arm 8q, as shown in panels a and b. The ratio of sequencing reads mapping to the major allele (more abundant allele) and minor allele was also measured (see methods). The left panel shows the expected relationship between absolute copy number and major/minor allele ratio. Note that higher level amplifications can involve a single allele or both alleles (see example inset to the right; blue = major allele, red = minor allele), producing several possible combinations. The right panel shows the observed relationship between absolute copy number and major/minor allele ratio. **d.** Copy number estimates from sequencing depth (CNVkit) concord with copy number estimates from Multiplex Ligation-dependent Probe Amplification (MLPA). Note that MLPA ratios become saturated at higher levels of copy number. **e.** Fluorescent In Situ Hybridization (FISH) over centromere 8 (left panel) and chromosomal arm 8q (right panel). The number of FISH signals over the chromosome 8 was counted from 50-300 cells, and the width of the black lines is proportional to the number of cells with a given copy number. Some cases have multiple black lines due to tissue heterogeneity (e.g. stromal cells and/or tumor subpopulations with distinct levels of 8q copy number). The copy number estimated from our next generation sequencing data is overlaid in red. *there were two melanoma areas in A73 with distinct copy number levels inferred from our sequencing data.

Figure S5.

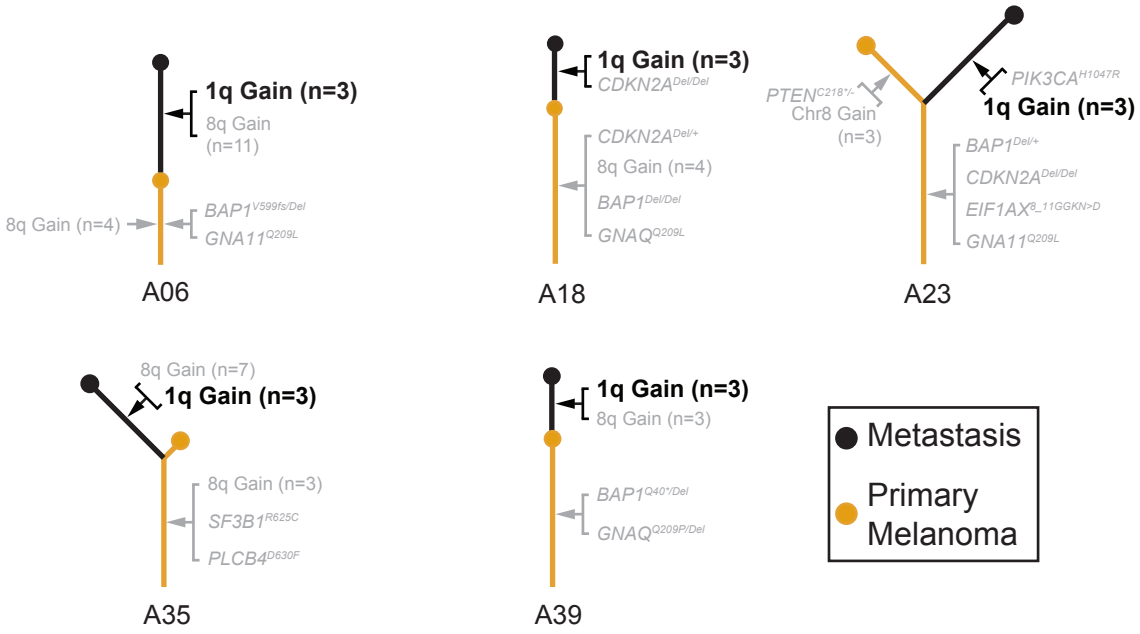

Figure S5. Gain of chromosomal arm 1q is common in uveal melanoma metastases. Phylogenetic trees illustrating that gain of chromosomal arm 1q exclusively occuring the metastasis. Refer to supplemental material for the detailed evolution of each case.

Figure S6.

a.

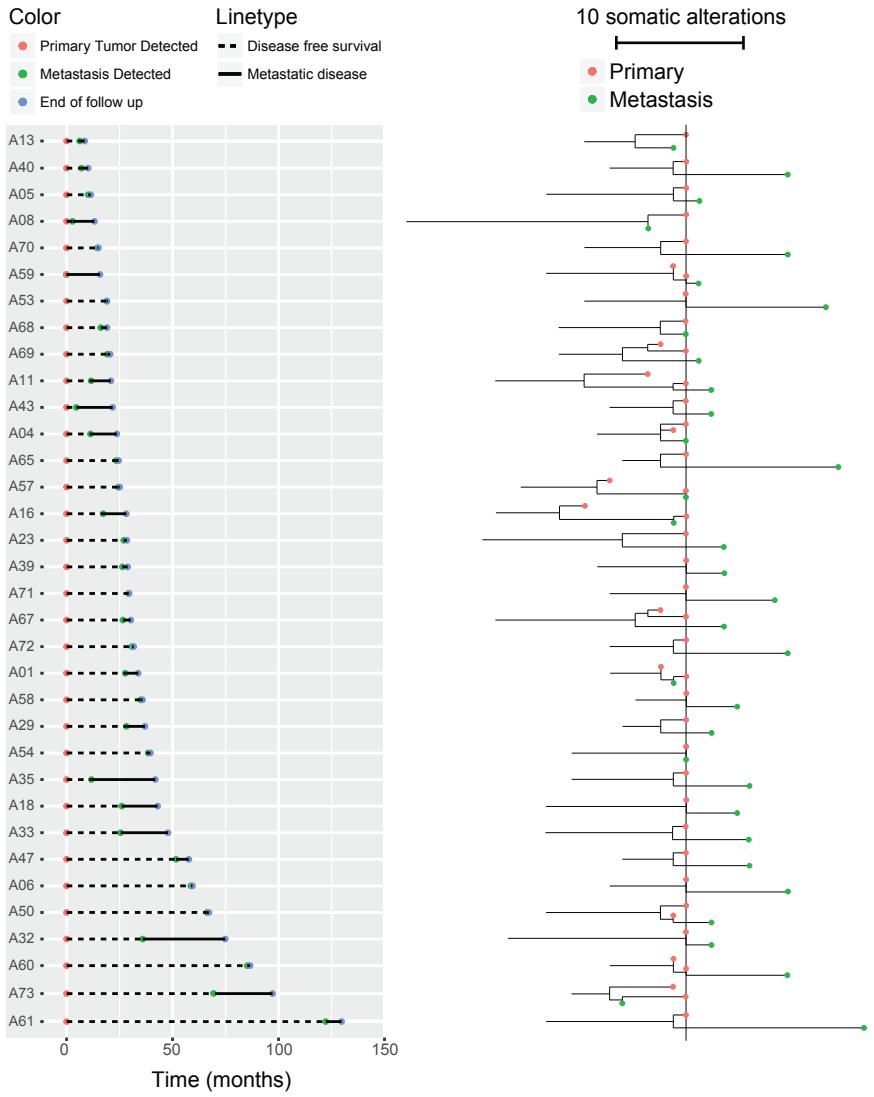

b. Pairwise correlations

R values	Disease-Free Survival	Survival After Metastasis	Overall Survival
a	0.34	-0.28	0.22
b	-0.17	-0.01	-0.16
c	-0.06	0.25	0.03
d	0.29	-0.31	0.16
e	0.22	0.01	0.21
f	0.17	-0.24	0.07

p values	Disease-Free Survival	Survival After Metastasis	Overall Survival
a	0.046	0.105	0.205
b	0.403	0.996	0.446
c	0.753	0.142	0.820
d	0.096	0.070	0.369
e	0.199	0.964	0.221
f	0.377	0.158	0.756

Adjusted p values	Disease-Free Survival	Survival After Metastasis	Overall Survival
a	0.836	1.000	1.000
b	1.000	1.000	1.000
c	1.000	1.000	1.000
d	1.000	1.000	1.000
e	1.000	1.000	1.000
f	1.000	1.000	1.000

Evolutionary features

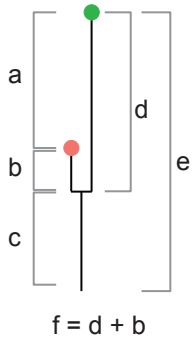

c.

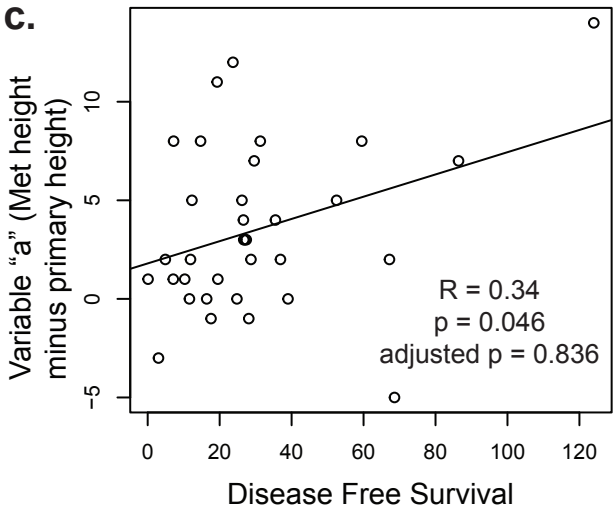

Figure S6. Correlations between phylogenetic features and clinical outcomes. a. The left portion depicts a timeline of clinical events for each case: detection of the primary tumor (pink dot, time = 0), disease-free survival (dotted line), detection of metastasis (green dot), survival after metastases (solid line), and death (blue dot). The right portion shows the phylogentic tree for each case, centered on the most genetically advanced portion of the primary tumor. **b.** Several measurements of the phylogenetic trees were taken (see legend at bottom of panel B) and recorded as variables a-f. We investigated correlations between these variables and disease-free survival, survival after metastasis, and overall survival. The pairwise correlation coefficients (R-values), p-values, and adjusted p-values (corrected for multiple hypothesis testing) are shown in the three tables. The highest correlation was between variable "a" and Disease-Free Survival (highlighted as yellow). **c.** A scatterplot depicting Variable "a" versus Disease-Free Survival is shown. The correlation was significant as a single comparison, but it did not remain significant after account for multiple hypothesis testing.